Forensic Science International 361 (2024) 112111

Contents lists available at ScienceDirect

Forensic Science International

journal homepage: www.elsevier.com/locate/forsciint

Bone mineral density and geometric morphometrics: Indicators of growth in the immature pars basilaris

Roxanne Thornton *, Mira G. Mendelow, Erin F. Hutchinson

School of Anatomical Sciences, Faculty of Health Sciences, University of the Witwatersrand, Johannesburg, South Africa

ARTICLE INFO

Keywords:
Pars basilaris
Fetal osteology
Geometric morphometrics
Bone mineral density

ABSTRACT

The pars basilaris forms a central component of the immature basicranium and owing to its resilience to post-mortem and taphonomic changes, holds significance across evolutionary, clinical, and forensic contexts. While size and shape parameters of the pars basilaris have been investigated, little is known about the influence of the underlying bone mineral density on the morphometry of this bone during growth. This study aimed to investigate the development and growth of the pars basilaris with specific reference to changes in bone density patterning and development of osteological features, during the prenatal and early postnatal periods of life. A total of 109 pars basilari were sourced from the Johannesburg Forensic Paediatric Collection, University of the Witwatersrand, South Africa. The study sample was subdivided into early prenatal (<30 gestational weeks), prenatal (30–40 gestational weeks) and postnatal (birth to 7.5 months) groups and micro-CT scanned to assess bone mineral density patterns across seven regions of interest. Size and shape changes were analysed using 11 digitized landmarks and geometric morphometrics. When comparing across age groups, the assessed dimensions increased with growth manifesting as a deepening at the anterior border of the foramen magnum, development of the lateral angles and widening of the bone at the lateral projections and spheno-occipital synchondrosis. However, no significant changes in the distribution of bone mineral density were observed. An appreciation of morphological changes and bone quality at specific growth sites in the pars basilaris is essential when analyzing remains of unknown provenance for the purposes of identification in disaster victim settings.

1. Introduction

The basicranium serves as a transitional platform for neurovascular structures communicating between the intracranial and extracranial spaces of the head and neck. As such, the development and growth of this area in the immature human skull has been central to age estimation investigations within the clinical and forensic contexts [5,6,11,18,24,25,26,41,53,71,72]. Age estimations of the immature cranial base in the forensic setting have thus far been collectively based on the ossification patterns of the individual skeletal elements, fusion and closure of the cranial sutures and changes in the flexion of the cranial base [9,29,73]. Owing to its role as the developing anterior border of foramen magnum, posterior border of the sphenooccipital synchondrosis and medially wedged between the developing petrous temporal bones (pars temporalis) [11,53,72], the pars basilaris holds significance across evolutionary, clinical, and forensic contexts [9,20,26,29,53,71,72]. Thus, it is important to fully understand the development and growth of the pars basilaris to appreciate how the changes in this bone may influence neighbouring areas of the basicranium with age.

Metric assessments of individual cranial base elements have gained popularity in terms of estimating age from immature skeletal remains [11,18,35,53,60,71,72,73]. While documenting the development of the occipital bone complex in an immature archaeological sample, Redfield [53] noted that individuals younger than 4 months prenatally had a long and narrow pars basilaris when compared to individuals at six months of postnatal life, where the width exceeded the length of the bone. Both Fazekas and Kosa [18] and Scheuer and Mclaughlin-Black [60] made similar observations, noting the width of the pars basilaris exceeds the length in individuals aged as early as five months postpartum across both modern and archaeological samples. While Redfield [53] documented the parameters for the length measurement of the pars basilaris, the width measurement was not as well defined. In contrast, Fazekas and Kosa [18] as well as Scheuer and Mclaughlin-Black [60] both documented the maximum length, sagittal length, and the width of the pars

* Correspondence to: School of Anatomical Sciences, Faculty of Health Science, Medical School Campus, University of the Witwatersrand, 7 York Road, Parktown, Johannesburg 2193, South Africa.
E-mail address: roxanne.thornton@wits.ac.za (R. Thornton).

https://doi.org/10.1016/j.forsciint.2024.112111
Received 13 November 2023; Received in revised form 27 May 2024; Accepted 12 June 2024
Available online 17 June 2024

basilaris. Nagaoka et al. [35], in an assessment of the immature pars basilaris in a modern Japanese sample, further expanded on the traditional length and breadth measurements to include an index of the pars basilaris as well as investigated the application of regression equations. While these studies assessed changes in the dimensions of the pars basilaris and made inferences around potential changes in the shape of the bone with growth based on their metric investigations [18,35,53,60], they did not directly assess shape or how the underlying changes in bone quality may influence dimensional change.

Niel et al. [44] analysed the maturation of the basioccipital bone using conventional computed tomography (CT) in the second and third trimesters of prenatal life (18–41 weeks of gestation) making use of two-dimensional landmark data and then analysing the sample using an elliptical fourier analysis and a principal component analysis. During the period of 18–26 weeks of gestation rapid changes in the overall shape of the pars basilaris were visualised, whereas shape changes were less visible between 27 and 41 weeks of gestation [44]. Zdilla et al. [72] utilized morphometric methods, which included both traditional measurements and geometric morphometrics, to assess ontogeny both from the size and shape perspective across individuals ranging in age between five months prenatally to five months postnatally. In the assessment of shape, a combination of photogrammetry, extended eigenshape and canonical variate analyses were performed to assess ontogenetic shape changes between age groupings [72]. Visualised shape changes included a transition from a narrow/elongated basiocciput shape with a mild concavity at the foramen magnum border in the fifth prenatal month, to a broad/stout shape with a pronounced concavity in the postnatal months and better visualised lateral projections postnatally [72]. While assessing shape through geometric morphometrics, both studies assessed this parameter within a limited two-dimensional scope.

While shape may often be linked to dimension related changes, there is limited information detailing what kind of alterations may be occurring in the quality of the underlying bone. Recently, changes in bone mineral density have been used as a potential indicator of the influence of biomechanical loading on bone quality across both immature and mature bone [22,34]. Hutchinson et al. [22] made use of changes in bone density as reflected across specified regions of interest in the lingual and buccal surfaces of the immature human mandible to highlight changes in bone development across the late prenatal and postnatal stages of growth. While changes in bone mineral density across the lingual surface were consistent with the progression of development and the biomechanical demand of the tongue, changes observed across the buccal/labial surface of the mandible appeared to accompany the advancing dental development [22]. In contrast to developing bone, Morris et al. [34] illustrated changes in bone mineral density across the adult human ear ossicles. The handle of the malleus, the incudo-stapedial joint and the insertion site for the tendon of stapedius had lower bone mineral densities when compared to adjacent articulation and non-attachment sites on the ossicular chain, which was attributed to biomechanical stress in response to sound conduction rather than ageing [34]. Thus, understanding potential changes in the underlying bone quality may further enhance our comprehension of size and shape changes in response to growth within a forensic context.

In biological and forensic anthropology, consideration of size and shape collectively is necessary when evaluating changes in immature skeletal elements, particularly for the purposes of age estimation in a forensic setting. While size serves as a reliable indicator of growth, it is in the subtle changes in shape and potentially bone density where the maturation of bony features is highlighted [22,44,71,72]. Thus size, shape and bone density should be considered collectively in the assessment of immature skeletal remains. Geometric morphometrics has been proven to be very valuable in the quantification and visualisation of subtle and often precise morphological variations in bone, through the aid of powerful visualization and statistical tools [62,33] In addition, micro-CT assessments of changes in the ratio of bone mineral density across developing osteological elements has recently proven useful in tracking and evaluating the changes in the development and growth of immature skeletal elements [22,34]. As such, it is envisioned that the findings from methods such as bone mineral density ratio plots may compliment the visualised changes in the morphology seen using geometric morphometrics. Thus, the aim of this study was to investigate the development and growth of the immature pars basilaris with specific reference to changes in bone density patterning, as well as development of osteological features using geometric morphometrics, during the prenatal and early postnatal periods of life.

2. Materials and methods

2.1. Sample

Human pars basilari were sourced from 90 fetal and infant individuals of unknown provenance from the Johannesburg Forensic Paediatric Collection (JFPC), Department of Forensic Medicine and Pathology, University of the Witwatersrand, South Africa. The JFPC is an ongoing humanitarian and scientific initiative, which aims to preserve and safeguard unidentified immature skeletal remains. Individuals included in the JFPC are unclaimed and unidentified decedents previously admitted to the Forensic Pathology Services for medicolegal examination. Under the [37] (Act No. 61 of 2003), the function of the Forensic Pathology Service in the Department of Health (DOH) in South Africa is the medico-legal investigation of unnatural death. Fetal and infant remains are admitted to the services in accordance with the Births and Deaths Registration Act no.51 of 1992 [7], section 12, and the Criminal Procedure Act, section 239 [10]. Ethical approval was granted through the Human Research Ethics Committee – Medical of the University of the Witwatersrand (Clearance certificate number: M210855).

Individuals were previously aged using dental radiographs taken with a Nomad portable x-ray scanner (Aribex, Charlotte, NC, USA) and age was assigned based on dental aging criteria proposed by Ref. [3]. Individuals with missing or damaged dentition were aged using anthropometric standards of the femur [64]. Subsequent to biological age estimations, the study sample was subdivided into early prenatal (younger than 30 gestational weeks), prenatal (30–40 gestational weeks) and postnatal (birth to 7.5 months) groups (Table 1).

Geometric morphometrics and bone mineral density (BMD) was used to evaluate sites of growth and articulation on the extracranial and intracranial surfaces of immature pars basilaris (Fig. 1). Individuals were excluded from analyses in the event of obvious developmental abnormalities or in cases where post-mortem damage was evident on bone surfaces, regions of interest or sites of landmark plotting. Therefore, sample sizes for each technique varied based on the above criteria. Biological sex was assigned at autopsy or via molecular assay depending on the condition of remains [66] (Table 1).

Table 1
Age and sex distribution of the sample applied to methods incorporated in the study (adapted from Ref. [67]).

Dental and Anthropometric age estimates	Biological Sex*		Method	
Age categories	Female	Male	Bone mineral Density (BMD)	Geometric Morphometrics
Early Prenatal (<30 gestational weeks)	13	11	18	25
Prenatal (30–40 gestational weeks)	12	13	19	37
Postnatal (Birth-7.5 months	20	9	22	27
Total (*N*)	45	33	59	89

* Biological sex determined at autopsy (when possible) or via molecular assay [66].

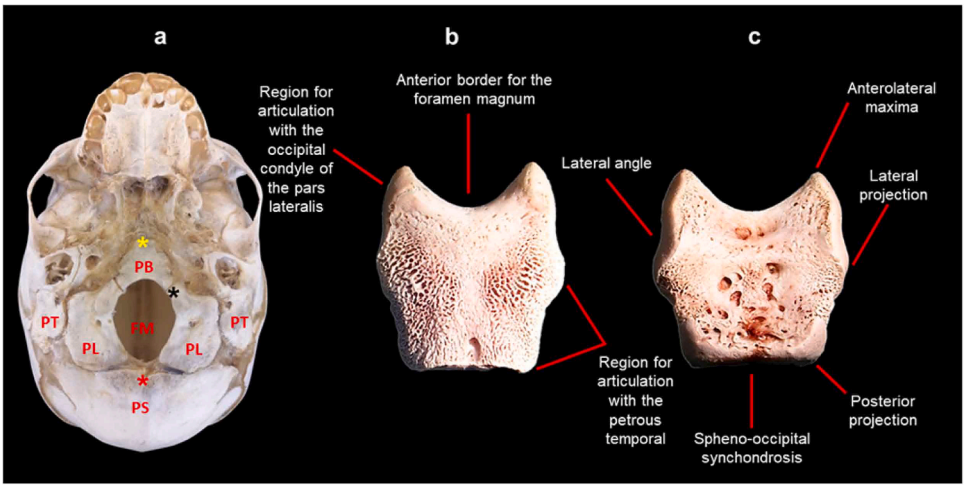

Fig. 1. :Prenatal basicranium representing osteological features of the Pars basilaris: a.) Extracranial view of the basicranium highlighting the PS: pars squama, PL: pars laterali, FM: foramen magnum, PB: pars basilaris, PT: pars temporalis and synchondroses* (Red: PIOS – posterior intra-occipital synchondrosis, Black: AIOS – Anterior intra-occipital synchondrosis and Yellow: SOS – Sphenoid-occipital synchondrosis. b.) Extracranial view of pars basilaris representing anterior border for the foramen magnum, region for articulation with the occipital condyle of the pars lateralis and region for articulation with the petrous temporal. c.) Intracranial view of the pars basilaris representing anterolateral maxima, lateral angle, lateral projection, posterior projection and spheno-occipital synchondrosis. Magnification (1.5x - 2.5x) performed on Nikon Stereomicroscope (SMZ1500, Japan).

2.2. Bone mineral density patterning

Bone mineral density (BMD) can be defined as the measure of inorganic mineral content present in bone [28]. The degree of mineral content is indicative of bone quality. To assess the portion of BMD at specific sites across the early prenatal, prenatal, and postnatal pars basilaris, elements were scanned using a Nikon XTH 225L micro-focus CT X-ray unit (Nikon Metrology, Leuven, Belgium) in the MIXRAD facility of the South African Nuclear Energy Corporation (NECSA).

Scanning parameters were set to 100 kV/100 μA and 100 μm as a means of standardising the scanning conditions across the sample. A 0.1 mm thick aluminium filter was used to approximate a homogeneous X-ray beam spectrum by removing the lower energy photons. Individual bones were securely mounted in OASIS floral foam (OASIS Floral Products, Gauteng, South Africa) and orientated in the intracranial view. A material of uniform composition was used as a density reference value across all scans. The mounted bones were then placed on to a rotating sample manipulator, which facilitated scanning at 360° and one-thousand projection images were obtained resulting in a good-quality scan. The scanning setup was optimised for highest spatial resolution where a resolution of between 0.023 and 0.050 μm was obtained. Subsequent to scanning, volume files were then reconstructed using NIKON CTPRO software (Nikon Metrology, Leuven, Belgium). After three-dimensional reconstruction, all the volume files were imported into VGStudio Max V2.2 (Volume Graphics GmbH, Heidelberg, Germany) for further analysis.

All imported volume files were subjected to a surface estimation analysis to allow for the selection of landmarks digitally. The orientation of the micro-CT slices of the pars basilaris elements were then standardised by aligning each slice to a pre-determined transverse reference plane. The transverse reference plane for each bone was established by selecting a minimum of three fiducial landmarks across the x, y, and z planes, along the extracranial view of the pars basilaris. Fiducial landmarks included the midline point on the 1. foramen magnum border, 2. the primary ossification site, and the 3. midline point on the spheno-occipital border (Fig. 2a–c).

Once the transverse reference plane was established, Micro-CT slices were aligned to this plane and density marker sites were selected and analysed across all surfaces of the pars basilaris to ascertain the bone density distribution. Each density marker site included a radius of 1.5 mm and thickness of 1.0 mm to assess bone density distribution across a series of slices. Density sites included the left and right anterolateral maxima (1,2), indent on the foramen magnum border (3), primary ossification site (4), left and right lateral projections (5 and 6)

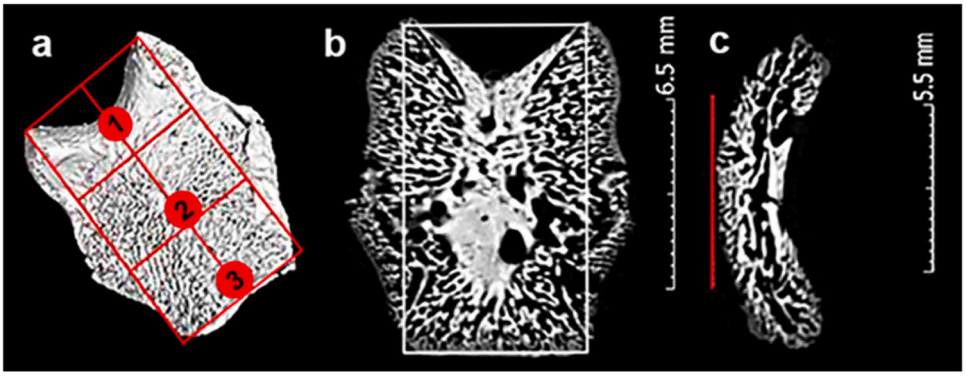

Fig. 2. Reference planes and density marker sites for the pars basilaris bone. Reference planes: a. 3D reconstruction of the early prenatal pars basilaris: red grid represents reference plane. Fiducial landmarks included the 1 (midline point on the foramen magnum border), 2 (the primary ossification site), and the 3 (midline point on the sphenooccipital border). b. Transverse section through the pars basilaris: white border represents reference plane. c. Coronal section through the pars basilaris: red line represents reference plane.

and the metaphyseal surface of the sphenooccipital synchondrosis (7) (Fig. 3a-c).

2.3. Geometrics morphometrics

To assess size and shape changes of the pars basilaris relative to each age group, a Microscribe® G2 digitiser (Immersion Corp., San Jose, California, USA) was used to digitize a series of fixed and floating landmarks. The general outline of the pars basilaris was digitized to study the overall shape of the bone relative to each age group. Each pars basilaris was positioned on Afffinis Perfect impressions morphometric putty (Coltene Holding co, Altstatten, Switzerland) with the intracranial surface facing towards the viewer (Fig. 4a).

A total of 11 landmarks associated with the intracranial surface were digitised and some of the selected landmarks overlapped with areas of the pars basilaris which were selected as density marker sites for bone density analysis (Fig. 3a–c). Of the digitised landmarks, six were fixed and five were floating (Table 2; Fig. 4a).

Fixed landmarks corresponded with distinct anatomical features, while floating landmarks were located along a curve or a border and used to define the shape of the structure. The shape of the bone was digitised in a clockwise pattern by recording the spatial x, y and z co-ordinates of each landmark and processed further using Excel (Microsoft, 2016) as well as Microscribe Utility software version 6.0.1 (Revware, 2011). Size was calculated using the three-dimensional landmarks data applied to a Pythagorean formula to find the distance between two landmarks [67,70].

The size of the pars basilaris was assessed by calculating the maximum width, sagittal length, and maximum length (Fig. 4b) [58,72]. Sagittal length is measured on the midline between the indent on the foramen magnum border and spheno-occipital synchondrosis (landmarks 2 and 7). Maximum length is the greatest distance between the anterolateral maxima and the posterior projection (landmarks 3 and 6). Maximum width is the greatest distance between the lateral projections (landmarks 5 and 9).

2.4. Data analysis

2.4.1. Bone mineral density patterning

The BMD patterning was assessed by means of calculating a bone mineral density ratio at each region of interest across the pars basilaris. To calculate the BMD ratio, the maximum grey value assessed at each region of interest point was used relative to the maximum grey value of the reference material included in each scan i.e., the maximum grey value of each assessment point was subdivided by the maximum grey value of the reference material. This resulted in the data for each assessment point being presented as a ratio, which allowed for further statistical analysis and comparisons of the bone mineral density

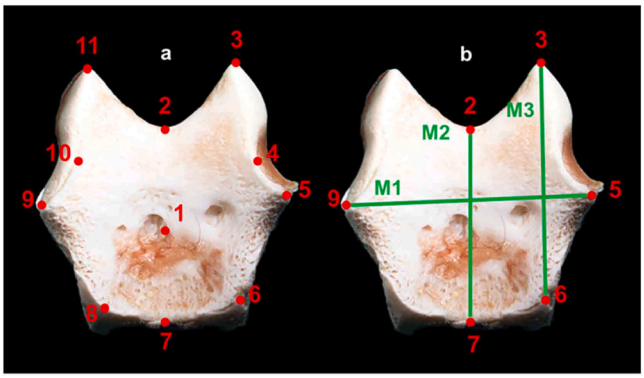

Fig. 4. Pars basilaris indicating the position of fixed and floating landmarks and measurements adapted from Schaefer et al. [58] and Zdilla et al. [72]. a. Intracranial view of pars basilaris with fixed landmarks: 3 and 11 (Anterolateral maxima), 5 and 9 (Lateral projections), 6 and 9 (Posterior projections). Floating landmarks: 1 (Centre), 2 (indent on the foramen magnum border), 4 and 10 (Lateral angles) and 7 (Spheno-occipital synchondrosis) b. Measurements to assess pars basilaris size: Maximum width (M1); Maximum length (M2); Sagittal length (M3). Magnification (1.5x - 2.5x) performed on Nikon Stereomicroscope (SMZ1500, Japan).

Table 2
Landmarks digitised on the pars basilaris.

Number	Osteological name	Description (Adapted from [58] and [72])
1	Centre	Centre of bone where the concavity is deepest
2	Indent on foramen magnum border	Deepest indentation on the posterior aspect, which forms the anterior border of the foramen magnum
3*/11*	Left/right anterolateral maxima	Most posterior projection on the right and left sides respectively
4/10	Left/right lateral angle	Midpoint on the exoccipital articular segment on the right and left sides respectively, which articulates with the pars lateralis
5*/9*	Left/right lateral projection	Lateral-most point between the exoccipital and temporal articular segments on the right and left sides respectively
6*/8*	Left/right posterior projection	Lateral edge of the spheno-occipital synchondrosis on the right and left sides respectively
7	Spheno-occipital synchondrosis	Anterior aspect of the bone perpendicular to the foramen, which articulates with the sphenoid bone

* Fixed landmark.

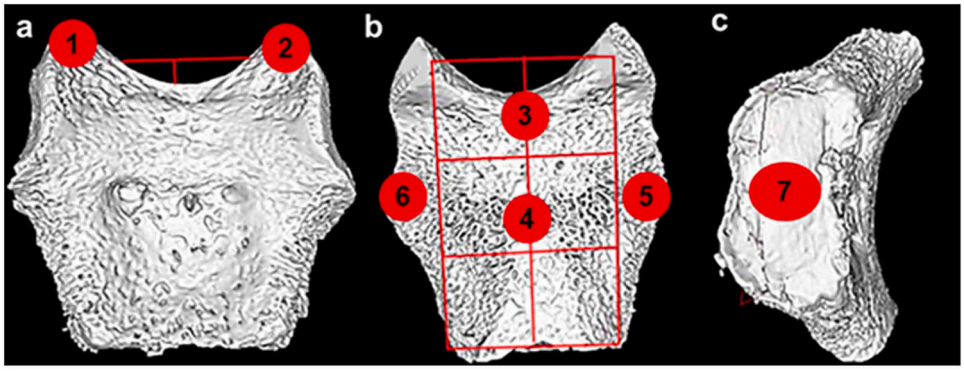

Fig. 3. Density marker sites for the pars basilaris bone. a. Intracranial view of the pars basilaris. b. Extracranial view of pars basilaris. c. Metaphyseal surface of the sphenooccipital synchondrosis. Density marker sites included: 1 (Right anterolateral maxima), 2 (Left anterolateral maxima), 3. (indent on the foramen magnum border), 4 (Primary ossification site), 5 (Right lateral projection), 6 (Left lateral projection), 7 (Spheno-occipital synchondrosis).

distribution values within individuals as well as across the sample. Each BMD ratio was thus used to show the pattern of change in BMD relative to other BMD sites across the pars basilaris and as such, served as a reflection of potential ossification of the bone. Descriptive statistics were applied to assess bone mineral density ratios associated with skeletal sites using Graphpad version 3.4.1 (Graphpad Software Inc., San Diego, California, USA).

2.4.2. Geometrics morphometrics

Size data was analysed using SPSS version 22 (Statistical Package for the Social Sciences, IBM Corporation., 2013). A Shapiro-Wilks test was run for each measurement (Fig. 3) to assess the distribution of the sample. As the sample was normally distributed, the appropriate means and standard deviations were calculated. A multivariate analysis of variance (MANOVA), with a Scheffe Post hoc was then used to assess the relationship between the age category relative to each measurement, where $p \leq 0.05$ was considered statistically significant. Principal component analysis was run using R studio developed for R software version 4.2.1 [51] using the software package Geomorph [1] to assess the level of variation across the sample.

A Generalised Procrustes Superimposition, which compared the relative position of each landmark while accounting for rotation and scaling, was used to study shape changes across the sample [70]. Landmark data was processed using Morphologika version 2.5 (University of York, United Kingdom) [48]. Wireframes were used to visualise changes in bone shape.

To account for inter- and intra-observer error, a sample of bones (inter-observer: n = 13; intra-observer: n = 17), across the age groups was randomly selected and the landmarks were digitised, and the measurements were recalculated. A Lin's concordance correlation was applied to the measurements were a value between 0.81 and 1.00 indicated a high level of repeatability [30].

3. Results

Inter- and intra-observer repeatability ranged between 90 % and 97 % for all geometric morphometric measurements. Reproducibility in plotting and determining the bone mineral density ratios at the specific sites of the pars basilaris was validated by an inter-observer error range of 81–99.4 %.

3.1. Bone mineral density patterning

No statistically significant differences were found between bone mineral density markers and biological age ranges. The mean values of the pars basilaris density sites were similar and variability of standard deviation within each density point was uniform. Density mean ratios were larger in the prenatal age range when compared to the postnatal age range for density points 1, 2 and 3. Density ratios were equal in the postnatal and prenatal age range. However, values for regions of interest were greater in the postnatal and prenatal age group when compared with the early prenatal age ranges respectively across the density points 4–7 (Fig. 5).

3.2. Geometric morphometrics

The measurements accessed resulted in a proportional increase between each age group for each measure. Statistically significant differences were observed across the maximum length ($p \leq 0.001$), maximum width ($p \leq 0.01$) and sagittal length ($p \leq 0.001$), when comparing the respective groups (Table 3).

When assessing the proportion of variation across the pars basilaris, PC1 accounted for majority of variation across the sample with 93.19 %, while PC2 accounted for 3.34 % percentage of variation. Principle component analysis of the pars basilaris indicated a moderate degree of variation in size and shape between the three age categories. A high degree of overlap was noted between the prenatal and postnatal group, indicating a lower degree of variation between these groups. A moderate degree of overlap between the prenatal and early prenatal groups was observed, indicating a higher degree of variation between the early prenatal and prenatal stage of development (Fig. 6). The variation in size and shape of the pars basilaris appear to be driven primarily by the changes in maximum width and length, with sagittal length contributing to a lesser extent (Fig. 6).

When comparing the wireframe data, the intracranial view of the early prenatal pars basilaris presented with a narrow and elongated shape (Fig. 7a), a more square-like shape in the prenatal age group (Fig. 7b) and a broad and defined hexagonal shape in the postnatal age group (Fig. 7c). The foramen magnum border (landmark 11–2–3) appeared deeper in prenatal cohort, compared to early prenatal elements (Fig. 7b). This deepening was more defined when comparing the postnatal and prenatal wireframes (Fig. 7c). The pars basilaris was deeper in the areas of the lateral angles (landmarks 4/10) and posterior projections (landmarks 6/8) relative to the centre (landmark 1) when comparing the early prenatal wireframes and prenatal wireframes (Fig. 6b and e) and prenatal and postnatal wireframes respectively (Fig. 7c and f).

A concavity at the centre of the bone (landmark 1) was present in the prenatal age range (Fig. 7e) and appeared to dissipate in the postnatal cohort (Fig. 7f). The pars basilaris appeared as shorter anterior-posteriorly along the midline (landmarks 2–1–7) in prenatal wireframes versus early prenatal wireframes when comparing the spheno-occipital synchondrosis surface (landmark 7) against the indent on the foramen magnum border (landmark 2) (Fig. 7b). The reduction in length between the indent on the foramen magnum border (landmark 2) and spheno-occipital synchondrosis (landmark 7) appeared more pronounced when comparing the prenatal and postnatal wireframes (Fig. 7c). The pars basilaris appeared shorter in both the intracranial and lateral views when comparing the postnatal group to the prenatal group (Fig. 7c and f). When comparing the early prenatal and prenatal

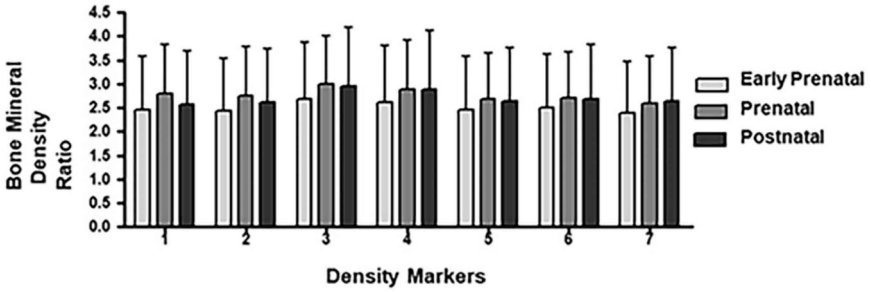

Fig. 5. Mean and standard deviation of bone mineral density ratio values for density markers across the pars basilaris. Early Prenatal (n = 18), Prenatal (n = 19), Postnatal (n = 22).1 (Right anterolateral maxima), 2 (Left anterolateral maxima), 3 (Indent on the foramen magnum border), 4) Primary ossification site), 5 (Right lateral projection), 6 (Left lateral projection), 7 (Spheno-occipital synchondrosis).

Table 3
Measurements (mean and standard deviation) of the pars basilaris for the Early Prenatal, Prenatal and Postnatal age ranges.

	Early Prenatal (n = 25) Mean (SD)	**Prenatal (n = 27)** Mean (SD)	**Postnatal (n = 37)** Mean (SD)	**Scheffe Post hoc (p≤)*** Early Prenatal vs. Prenatal	Prenatal vs. Postnatal
Maximum Width	7.93 (1.49)	10.41 (1.81)	13.20 (1.68)	0.001	0.001
Maximum Length	8.89 (1.31)	11.08 (1.44)	13.16 (1.58)	0.001	0.001
Sagittal length	8.22 (1.07)	9.64 (0.92)	10.88 (1.04)	0.001	0.001

* Statistically significant: $p \leq 0.05$.

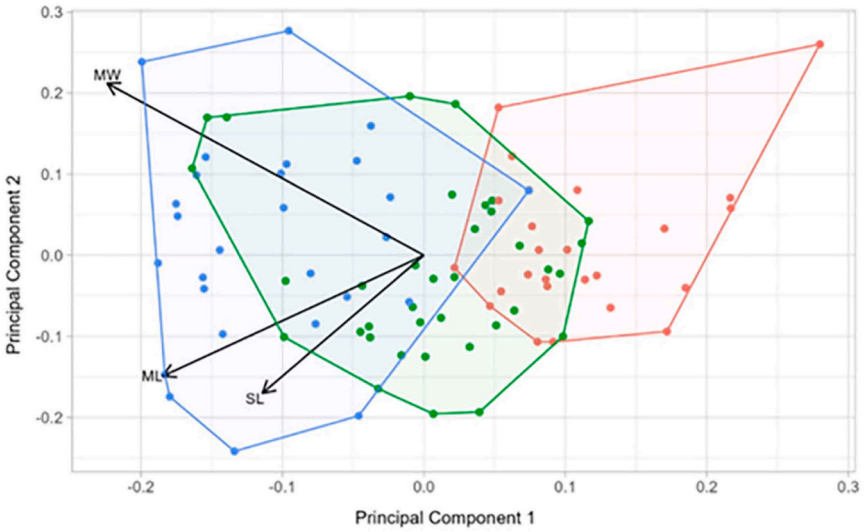

Fig. 6. Principal Component Analysis (PCA) assessing the degree of variation in the size of the pars basilaris, and distribution of individuals included in the sample. Age categories: early prenatal (red, less than 30 gestational weeks), prenatal (green, 30 gestational weeks – birth) and postnatal (blue, birth – 7.5 months postnatal). PC 1 represents size and shape. PC 2 represents shape only. The length of the line reflects the degree of inference of measurements on the size and shape variance in the sample relative to growth.

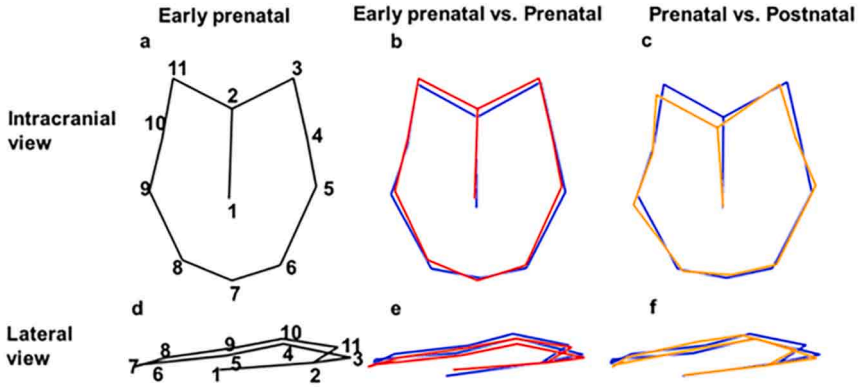

Fig. 7. Wireframes illustrating the intracranial and lateral shape of the pars basilaris. Intracranial surface: a. Early prenatal stage: less than 30 gestational weeks. b. Prenatal (blue)intracranial surface wireframe superimposed on Early Prenatal (red) intracranial surface wireframe. c. Postnatal (orange) intracranial surface wireframe superimposed on Prenatal (blue) intracranial surface wireframe. Lateral view: d. Early prenatal stage. e. Prenatal (blue) lateral view wireframe superimposed on Early Prenatal (red) lateral view wireframe. f. Postnatal (orange) lateral view wireframe superimposed on Prenatal (blue) lateral view wireframe. Numbers 1 – 11 indicate landmarks.

wireframes, the bone presented as wider, particularly in the regions of the lateral projections (landmarks 5 and 9) in the intracranial view (Fig. 7b and c). The widening of the pars basilaris is further illustrated in the lateral view as the distance between the centre of the bone (landmark 1) and the lateral projections (landmarks 5 and 9) appeared greater when comparing the early prenatal (Fig. 7d) against the other assessed groups (Fig. 7e and f).

In addition to the wider appearance at the lateral projections, the distance between the posterior projections (landmarks 8 and 6) appeared greater in the prenatal versus the early prenatal wireframes (Fig. 7b and e). In the lateral view, the postnatal posterior projections (landmark 8 and 6) (Fig. 7f), appear to adopt a similar profile to what was observed in the early prenatal group (Fig. 7d and e).

4. Discussion

Anthropometric criteria obtained from cranial and postcranial skeletal elements assist in determining viability [11,42,59] of unclaimed

and unidentified immature remains. Ascertaining age and viability of fetal remains is a core objective during the medicolegal autopsy. This is particularly important under the [37] (Act No.61 of 2003), concerning fetal and infant deaths in South Africa. Medicolegal investigations include establishing medical and legal viability of the fetus ($\leq$ 26 gestational weeks) during the routine medicolegal autopsy, as well as determining separate existence and personhood.

Establishment of viability and age at death at autopsy is reliant on body weight and external measurements of soft tissues [27], which refer to developmental charts, ossification centres and histological examination [17,19,32,61]. However, the condition of the remains compromises the validity of soft tissue age estimation [50]. In circumstances where the cause of death is unascertained, and the accuracy of soft tissue age estimation is questionable, fetal, and infant remains are often unidentified. Thus, ancillary biological anthropological assessments are employed.

The pars basilaris has proven to be useful in estimating viability and separate existence. The pars basilaris is thought to be highly resilient to post-mortem and taphonomic changes, and as, such the age-related changes in the size and shape have been incorporated in age-at-death estimations within the medico-legal settling [4,18,35,43,53,60,65]. The current study expands on the existing body of knowledge by providing novel information on uniform bone mineralization during gestation and the first year of life. In addition, data generated demonstrates size and shape variation of the immature pars basilaris from a forensic South African sample. Findings include significant differences in anthropometric measurements when comparing the postnatal group against the prenatal and early prenatal age groups respectively. When comparing age groups, the increase in the assessed dimensions manifested as a deepening at the anterior border of the foramen magnum, development of the lateral angles and widening of the bone at the lateral projections and spheno-occipital synchondrosis. The observed changes in shape may be attributed to an increase in the overall dimensions of the bone. While size and shape appeared to change across the age groups, no significant changes in the distribution of bone mineral density, were observed. The absence of significant change in bone mineral density, across the pars basilaris in the current study suggests that ossification remains stable during late gestation and the first year of life.

The uniform bone mineral density of the pars basilaris observed in the current study is in contrast to previous reports on the immature mandible [22], ear ossicles [34] and vertebral bones [47,57], when examined through the lens of potential biomechanical factors associated with growth [12,21,40,69,75]. The results from the current study indicate minimal biomechanical influence on the mineralization across the entirety of the pars basilaris during the fetal and postnatal stage of development. However, extraneous variables such as maternal health and environmental factors [36] may have contributed to the variability in results. The absence of significant differences in bone mineral density coupled with the biometric findings in the current study supports the hypothesis of the basicranial skeleton undergoing uniform development and growth across its entirety in support of brain development during the prenatal period of life [39,73]. The current study data serves as a baseline on bone surface mineralization of the human pars basilaris. It is hypothesized that the lack of statistically significant variants in bone density ratio suggests that the ossification process is limited in its influence on morphological development [25].

A potential reason for minimal variation in the bone mineral density observed across the pars basilaris in the current study may be explained by the mineralization being delayed due to changes in the size of the bone with growth as seen by the significant increase in all measurements. The overall shape of the pars basilaris transitioned from narrow and elongated in the early prenatal age group to square-like in the prenatal age groups and finally a broad and hexagonal shape in the postnatal group. The absence of statistically significant differences in density ratios within the three age groupings examined raises questions around the potential determinants of size and shape variants during gestation and neonatal life. One plausible determinant is the influence of neighbouring anatomy and future articulation with corresponding osteological components of the cranial base. The sequence of fusion with the corresponding pars lateralis, pars temporalis and sphenoid bone may influence linear growth.

When considering the observed increases in the assessed dimensions in the current study, geometric morphometric data indicated that maximum width is the primary driving force behind these changes between the age groups. The influence of the maximum width was evident through an increase in distance between the centre of the bone (landmark 1) and the lateral projections (landmark 5 and 9). In addition, the increase in maximum width found in the prenatal and postnatal sample, may be associated with the concavity at the centre of the bone (landmark 1), the deepening of the indent on the foramen magnum border (landmark 2) and decreased distance between the spheno-occipital border (landmark 7) and the indent on the foramen magnum border (landmark 2). The observed changes in the width may also be the result of growth of the lateral border of the pars basilaris to accommodate articulation with the jugular and condylar limb of the pars lateralis, as is evident by the deepening of the lateral angles (landmarks 4 and 10). These observed changes produce a hexagonal shape which is suggestive of a postnatal age range. The results in the current study suggest that the dimension between the lateral projections (landmarks 5 and 9), may be of the value for age estimation of late prenatal or postnatal individuals [42,65].

The increase in the maximum length was found to be consistent across the sample and serves as a characteristic linear measurement for prenatal individuals [63,65]. An increase in the maximum length dimension corresponds with the development of the anterior intra-occipital synchondrosis (landmark 3/11) and expansion of the posterior projections for the spheno-occipital synchondrosis (landmark 6/8). The wireframe data in the current study indicated a deepening of the indent on the foramen magnum border (landmark 2) in conjunction with the increase in dimensions between the anterolateral maxima (landmark 3/11) and the widening of the border of the spheno-occipital synchondrosis (landmark 6–7–8) in the prenatal and postnatal samples. This data suggests that there is significant growth along the sagittal axis of the basicranium during the prenatal period of development. These results indicate a functional relationship with the developing hypoglossal region of the pars lateralis and petrous part of the temporal bone [59] and immature sphenoid bone [25,31]. Furthermore, the current study data agrees with the proportional changes observed in a French sample with respect to maximum length [42]. Therefore, these results suggest that maximum length and width are advancing simultaneously to produce characteristic shapes observed in the prenatal and postnatal samples. This is particularly relevant when considering the supportive role of the pars basilaris in forming the anterior aspect of the foramen magnum [55].

The sagittal length measurement was found to be less impactful on size and shape in the older age groups, and as such, was deemed to be more indicative of a younger individual within the early prenatal stage of development when assessing the sample variance. In agreement with previous reports [60,68,72], sagittal length indicates an individual younger than 28 weeks in utero and suggest that elongation in an anterior-posterior direction is of prime importance prior to 7 gestational months. The morphology of the early prenatal pars basilaris represents a characteristic triangular shape, with the border for the foramen magnum (landmarks 11–2–3) appearing as a narrow v-shape and the border for the spheno-occipital border (landmarks 8–7–6) appeared as angled and pointed. As the pars basilaris ossifies from a cartilaginous precursor [11], the early prenatal pars basilaris presented as a thin plate of ossified tissue surrounded by cartilage in the current study. This observation agrees with previous reports concerning ossification during gestation [45,46], as the cartilaginous tissue provides a blueprint for development and growth as well as protects newly ossified tissue. It is hypothesized that during the early prenatal stage of development, the shape and size

of pars basilaris is primarily driven by intrinsic genetic programming [24,25,41].

The vasculature associated with the posterior cranial base may influence the geometry of the pars basilaris. The deepening of the centre of the bone (landmark 1) in the prenatal sample and the deepening of the region between the posterior projections (landmarks 6/8) relative to the centre of the bone (landmark 1) may be indicative of support for vasculature of the basilar plexus and pharyngeal venous plexus during late gestation [38,71,74]. Furthermore, the growth of the pharynx and larynx may influence the morphological variants (Lieberman and McCarthy, 1998; [25]), due to the anatomical relationship of the constrictor muscles of nasopharynx and the external basicranium [2,49,52]. This is particularly relevant when considering force applied over time due to the swallowing mechanism *in utero* and after birth. These results suggest a co-dependent relationship between the osteology and associated soft tissues, which has been previously suggested despite brain development advancing prior to skull ossification [15,56,54].

The findings of the current study aid our understanding of shape changes during the gestational period as well as assist in signposting the development of key maturation stages, which has the potential to aid in age at death estimations and forensic identification of immature individuals. The use of the immature pars basilaris for estimation of age at death is favourable due to dynamic shape changes and rapid growth during gestation and the postnatal period. Individuals included in this sample represent an ongoing social and public health problem in South Africa [16,23,66], as remains originate from a forensic setting and as such the circumstance of death associated with these individuals included illegal abortion, concealment of birth and homicide. The unknown provenance of the skeletal remains included in the sample is a limitation. Records on the clinical history of the mother and information relating to Last Menstrual Period (LMP) are unavailable as individuals were admitted to forensic pathology services as unclaimed and unidentified. However, ancillary testing in the form of skeletal age estimation has been shown to be incredibly accurate and valid [11]. This is due to the rapid development, ossification rate and remodelling of bone tissue *in utero*. In addition, the sample did not originate from a clinical setting and cases included in the sample are not representative of therapeutic abortions or deaths due to pathology (as per the autopsy report). Furthermore, the osteology of pars basilari included in the sample were inspected for abnormalities prior to inclusion.

Forensic remains are often discovered at an advanced stage of decomposition with evidence of predation or head trauma [16,23,64], which compromises the newly formed osteology at the borders of fragile skeletal elements. Postmortem modification was observed at the anterolateral maxima (landmark 3/11), lateral projections (landmark 5/9) and spheno-occipital synchondrosis (6−7−8). These sites correspond with the expansion of the bone as demonstrated by the anthropometric results. Therefore, an appreciation of morphological changes at specific sites of growth is essential when analyzing remains of unknown provenance with little or no ante-mortem data. This is particularly relevant when remains are fragmentary and for the purposes of human identification in disaster victim settings [8,13,14].

5. Conclusion

Forensic identification of the human fetal and neonatal remains is reliant on the parameter of age [11]. The homologous nature of the pars basilaris allows for method improvement and validation across populations groups. The current study utilized three-dimensional landmark data generated using geometric morphometrics, to provide information on the subtle changes in shape, which influences global change [44,72]. Therefore, the development and growth of the pars basilaris during the prenatal and postnatal stage is gradual and dependent on the dynamic changes observed from fixed landmark data, which supports neural tissue [39,41]. This is evident by changes associated with biological age observed across the medial border for the foramen magnum as well as sites of articulation with the pars laterali, pars temporalis and post sphenoid bone. Development of osteomorphic stages of development, which are reliant on these shape dynamics but discriminate against altered growth states would prove advantageous within forensic settings and negate possible biases in age estimation [43] There are often discrepancies in the rate of maturation concerning differing tissue sources (i.e., dental, or skeletal) [64]. A combination of methods which are sensitive to a minority populations and age ranges is considered best practice when employing new reference material within medico-legal settings.

CRediT authorship contribution statement

Erin Frances Hutchinson: Writing – review & editing, Writing – original draft, Validation, Supervision, Software, Resources, Project administration, Methodology, Formal analysis, Conceptualization. **Mira Grace Mendelow:** Writing – original draft, Visualization, Methodology, Investigation, Formal analysis, Data curation. **Roxanne Thornton:** Writing – review & editing, Writing – original draft, Visualization, Validation, Supervision, Resources, Project administration, Methodology, Investigation, Formal analysis, Data curation.

Declaration of Competing Interest

None

Acknowledgements

This work was made possible through funding from the University of the Witswatersrand Research office. The authors would like to acknowledge the Johannesburg Forensic Paediatric Collection, Department of Forensic Pathology and Medicine, University of the Witwatersrand. Bone mineral density data was collected as part work funded by Sandiswa Imbewu grant (Upando Ubungqina, Rhodes University, South Africa) and as such the authors would like to thank Professor Adrienne Edkins, Rhodes University for her support and agreement in publishing bone mineral density data. The authors declare no conflict of interest.

References

[1] D.C. Adams, M.L. Collyer, A. Kaliontzopoulou, E.K. Baken, Geomorph: Software for geometric morphometric analyses, R. Package Version (2022). ⟨https://cran.r-project.org/package=geomorph⟩, 4.0.4. [Software]. [Accessed: 29.08.22]. Available.
[2] C. Alkan, P. Coe, E. Eichler, Development and evolution of the pharyngeal apparatus, WIREs Dev. Biol. 23 (3) (2014) 403–418.
[3] S.J. AlQahtani, M.P. Hector, H.M. Liversidge, Brief communication: The London atlas of human tooth development and eruption, Am. J. Phys. Anthropol. 142 (3) (2010) 481–490.
[4] G.A. Badiu, E. Tarta-Arsene, A.I.T. Ispas, A. Niculae, A. Baciu, L. Stroică, Estimation of the age from fetal occipital bone. Revista Română de Anatomie funcţională şi clinică, macro- şi microscopică ş, i De. Antropol. 18 (3) (2019) 165–168.
[5] M. Bastir, A. Rosas, P. O'Higgins, Craniofacial levels and the morphological maturation of the human skull, J. Anat. 209 (5) (2006) 637–654.
[6] S. Bhatnagar, J. Iwanaga, T. Decater, M. Loukas, R.S. Tubbs, Foramen magnum variant with elongation of the Anterior Notch, Cureus 12 (6) (2020) 10–13.
[7] Birth and Deaths Registration Act, 1992, No.51, s. 12, Cape Town: University of Pretoria and South African Legal Information Institute, available: ⟨http://www.chr.up.ac.za/undp/domestic/docs/legislation_55.pdf⟩. (accessed 16 June 2018).
[8] S. Blau, C.A. Briggs, The role of forensic anthropology in Disaster Victim Identification (DVI), Forensic Sci. Int. 205 (1-3) (2011) 29–35.
[9] H.F.V. Cardoso, J. Gomes, V. Campanacho, L. Marinho, Age estimation of immature human skeletal remains using the post-natal development of the occipital bone, Int. J. Leg. Med. 127 (5) (2013) 997–1004.
[10] Criminal Procedure Act, 1977, No. 51, s.239. Cape Town: Juta and Company, available: ⟨http://www.justice.gov.za/legislation/acts/1977-051.pdf⟩. (accessed 16 June 2008).
[11] C. Cunningham, L. Scheuer, S. Black. Developmental Juvenile Osteology, 2nd edn, Elsevier: Academic press publication, London, 2016.
[12] P. D'Amelio, G.L. Panattoni, G.C. Isaia, Densitometric study of Human Developing Dry Bones: A Review, J. Clin. Densitom. 5 (1) (2002) 73–78.

[13] A. Dahal, D. McNevin, M. Chikhani, J. Ward, An interdisciplinary forensic approach for human remains identification and missing persons investigations, WIREs Forensic Sci. 5 (4) (2023) e1484.
[14] H.H. de Boer, S. Blau, T. Delabarde, L. Hackman, The role of forensic anthropology in disaster victim identification (DVI): recent developments and future prospects, Forensic Sci. Res. 4 (4) (2018) 303–315.
[15] C. Delteil, E. Lesieur, L. Tuchtan, A. Carballeira Alvarez, K. Chaumoître, B. Saliba, P. Adalian, M.D. Piercecchi-Marti, Study of the growth and shape of the brain and cranial base during the first two years of life, Morphologie 105 (348) (2021) 45–53.
[16] L. du Toit-Prinsloo, C. Pickles, Z. Smith, J. Jordaan, G. Saayman, The medico-legal investigation of abandoned fetuses and newborns—a review of cases admitted to the Pretoria Medico-Legal Laboratory, South Africa, Int. J. Leg. Med. 130 (2) (2016) 569–574.
[17] J. Ersch, T. Stallmach, Assessing gestational age from histology of foetal skin: an autopsy study of 379 foetuses, Obstet. Gynecol. 94 (5) (1999) 753–757.
[18] Fazekas, I.G., Kosa, F. (1978). Forensic Fetal Osteology. Budapest: Akadémiai Kiadó,1-287.
[19] E. Gilbert-Barness, D.E. Debich-Spicer, Handbook of Pediatric Autopsy Pathology, Humana Press, New Jersey, 2010, pp. 7–74.
[20] J.T. Goodrich, Skull base growth in craniosynostosis, Childs Nerv. Syst. 2005 21 (10) (2005) 871–879.
[21] C.J. Hernandez, T.M. Keaveny, A biomechanical perspective on bone quality, Bone 39 (6) (2006) 173–1181.
[22] E.F. Hutchinson, M. Farella, J. Hoffman, B. Kramer, Variations in bone density across the body of the immature human mandible, J. Anat. 230 (5) (2017) 679–688.
[23] R. Jacobs, N. Hornsby, S. Marais, Unwanted pregnancies in Gauteng and Mpumalanga provinces, South Africa: examining mortality data on dumped aborted fetuses and babies, South Afr. Med. J. 104 (12) (2014) 864–869.
[24] N. Jeffery, A high-resolution MRI study of linear growth of the human fetal skull base, Neuroradiology 44 (4) (2002) 358–366.
[25] N. Jeffery, F. Spoor, Ossification and midline shape changes of the human fetal cranial base, Am. J. Phys. Anthropol. 123 (1) (2004) 78–90.
[26] A. Klocke, R.S. Nanda, B. Kahl-Nieke, Role of cranial base flexure in developing sagittal jaw discrepancies, Am. J. Orthod. Dentofac. Orthop. 122 (4) (2002) 386–391.
[27] B. Knight, P. Saukko. Knights Forensic Pathology, 3rd ed., Oxford University Press, New York, 2004.
[28] E.F. Kranioti, A. Bonicelli, J.G. García-donas, Bone-mineral density: clinical significance, methods of quantification and forensic applications, Res. Rep. Forensic Med. Sci. 9 (2019) 9–21.
[29] D.E. Lieberman, R.C. McCarthy, The ontogeny of cranial base angulation in humans and chimpanzees and its implications for reconstructing pharyngeal dimensions, J. Hum. Evol. 36 (5) (1999) 487–517.
[30] L. Lin, A concordance correlation coefficient to evaluate reproducibility, Biometrics 45 (1) (1989) 255–268.
[31] N. Mano, B. Wood, L. Oladipupo, R. Reynolds, J. Taylor, E. Durham, J.J. Cray, C. Vinyard, V.B. DeLeon, T.D. Smith, The chondrocranial key: Fetal and perinatal morphogenesis of the sphenoid bone in primates, Vertebr. Zool. 71 (2021) 535–558.
[32] L.L. Maroun, N. Graem, Autopsy standards of body parameters and fresh organ weights in non-macerated and macerated human foetuses, Pediatr. Dev. Pathol. 8 (2006) 204–217.
[33] P. Mitteroecker, P. Gunz, Advances in Geometric Morphometrics, Evolutionary Biology 36 (2009) 235–247.
[34] C. Morris, B. Kramer, E.F. Hutchinson, Bone mineral density of human ear ossicles: an assessment of structure in relation to function, Clin. Anat. 31 (8) (2018) 1158, 2018.
[35] T. Nagaoka, Y. Kawakubo, K. Hirata, Estimation of fetal age-at-death from the basilar part of the occipital bone, Int. J. Leg. Med. 126 (5) (2012) 703–711.
[36] R. Namgung, R.C. Tsang, Factors affecting newborn bone mineral content: in utero effects on newborn bone mineralization, Proc. Nutr. Soc. 59 (2000) 55–63.
[37] National Health Act, 2003, No.61, Cape Town: Government Gazette, available: ⟨http://www.chr.up.ac.za/undp/domestic/docs/legislation_55.pdf⟩. (accessed 16 June 2018).
[38] S.R. Nayak, V.V. Saralaya, L.V. Prabhu, M.M. Pai, A. Krishnamurthy, Clinical significance of a mysterious clival canal, Rom. J. Morphol. Embryol. 48 (4) (2007) 427–429.
[39] W.R. Nemzek, H.A. Brodie, S.T. Hecht, B.W. Chong, C.J. Babcook, J.A. Seibert, MR, CT, and plain film imaging of the developing skull base in fetal individuals, Am. J. Neuroradiol. 21 (9) (2000) 1699–1706.
[40] K. Neumann, A. Moegelin, M. Temminghoff, R.J. Radlanski, A. Langford, M. Unger, R. Langer, J. Bier, 3D-computed tomography: a new method for the evaluation of fetal cranial morphology, J. Craniofacial Genet. Dev. Biol. 17 (1) (1997) 9–22.
[41] X. Nie, Cranial base in craniofacial development: Developmental features, influence on facial growth, anomaly, and molecular basis, Acta Odontol. Scand. 63 (3) (2005) 127–135.
[42] M. Niel, P. Adalian, New models to estimate fetal and young infant age with the pars basilaris biometry, Forensic Sci. Int. 342 (2023) 111531.
[43] M. Niel, K. Chaumoître, P. Adalian, Age-at-death estimation of fetuses and infants in forensic anthropology: a new "coupling" method to detect biases due to altered growth trajectories, Biology 11 (2) (2022) 200.
[44] M. Niel, K. Chaumoître, J. Corny, L. Lalys, P. Adalian, Maturation of the human foetal basioccipital: quantifying shape changes in second and third trimesters using elliptic Fourier analysis, J. Anat. 235 (1) (2019) 34–44.
[45] C., R. Noback, The developmental anatomy of the human osseous skeleton during the embryonic fetal and circumnatal periods, Anat. Rec. 88 (1944) 99–125.
[46] C.R. Noback, G.G. Robertson, Sequences of appearances of ossification centers in the human skeleton during the first five prenatal months, Am. J. Anat. 89 (1951) 1–28.
[47] S. Nuzzo, C. Meneghini, P. Braillon, R. Bouvier, S. Mobilio, F. Peyrin, Microarchitectural and physical changes during fetal growth in human vertebral bone, J. Bone Miner. Res. 18 (4) (2003) 760–768, 2003.
[48] O'Higgins, P., Jones, N. Morphologika: Tools for statistical shape analysis.2006. Version 2.5. [Software]. [Accessed: 27.05.22]. Available: ⟨http://sites.google.com/site/hymsfme/resources⟩.
[49] A.S. Pagano, J.T. Laitman, Three-dimensional geometric morphometric analysis of the nasopharyngeal boundaries and its functional integration with the face and external basicranium among extant hominoids, Anat. Rec. 298 (1) (2015) 85–106.
[50] M.D. Piercecchi-Marti, P. Adalian, A. Liprandi, D. Figarella-Branger, O. Dutour, G. Leonetti, Fetal visceral maturation: a useful contribution to gestational age estimation in human fetuses, J. Forensic Sci. 49 (5) (2004) 912–917.
[51] R Core Team, R: A Language and Environment for Statistical Computing, in: Https://www.R-project.org., R Foundation for Statistical Computing, Vienna, 2022.
[52] R. Rai, J. Iwanaga, G. Shokouhi, M. Loukas, M.M. Mortazavi, R.J. Oskouian, R. S. Tubbs, A comprehensive review of the clivus: anatomy, embryology, variants, pathology, and surgical approaches, Child's Nerv. Syst. 34 (8) (2018) 1451–1458.
[53] A. Redfield, A new aid to aging immature skeletons: development of the occipital bone, Am. J. Phys. Anthropol. 33 (2) (1970) 207–220.
[54] S.R. Rengasamy Venugopalan, E. Van Otterloo, The skull's girder: A brief review of the cranial base, J. Dev. Biol. 9 (1) (2021) 1–17.
[55] G.D. Richards, R.S. Jabbour, Foramen magnum ontogeny in homo sapiens: a functional matrix perspective, Anat. Rec. 294 (2) (2011) 199–216.
[56] J.T. Richtsmeier, K. Flaherty, Hand in glove: Brain and skull in development and dysmorphogenesis, Acta Neuropathol. 125 (4) (2013) 469–489.
[57] B.L. Salle, P. Braillan, F.H. Glorieux, J. Brunet, E. Cavero, P.J. Meunier, Lumbar bone mineral content measured by dual energy X-ray absorptiometry in newborns and infants, Acta Pædiatrica 81 (12) (1992) 953–958.
[58] M. Schaefer, S. Black, L. Scheuer, Juvenile Osteology: A Laboratory and Field Manual, Elsevier, 2009.
[59] L. Scheuer, S. Black, The Juvenile Skeleton, Elsevier, London, 2004.
[60] L. Scheuer, S. Maclaughlin-black, Age estimation from the pars basilaris of the fetal and juvenile occipital bone, Int. J. Osteoarchaeol. 4 (1994) 377–380.
[61] T.G. Schwär, J.D. Loubser, J.A. Olivier, The Forensic ABC in Medical Practice, HAUM Education Publishers, Pretoria, 1988, pp. 289–313.
[62] D. Slice, Geometric morphometrics, Annu. Rev. Anthropol. 36 (2007) 261–281.
[63] D.E. Smith, L.T. Humphrey, H.F. Cardoso, Age estimation of immature human skeletal remains from mandibular and cranial bone dimensions in the postnatal period, Forensic Sci. Int. 327 (2021) 110943.
[64] Thornton, R. (2018). Towards a biological profile of South African perinatal remains: Osteological and genetic perspectives. Rhodes University, Grahamstown.
[65] R. Thornton, A.L. Edkins, E.F. Hutchinson, Contributions of the pars lateralis, pars basilaris and femur to age estimations of the immature skeleton within a South African forensic setting, Int. J. Leg. Med. 134 (3) (2019) 1185–1193.
[66] R. Thornton, E.F. Hutchinson, A.L. Edkins, PCR based method for sex estimation from bone samples of unidentified South African fetal remains, Forensic Sci. Int.: Rep. 4 (2021) 100248.
[67] R. Thornton, M.G. Mendelow, E.F. Hutchinson, Assessing the morphology and bone mineral density of the immature pars lateralis as an indicator of age, Int. J. Leg. Med. 138 (2) (2023) 1–20.
[68] M.W. Tocheri, J.E. Molto, Aging fetal and juvenile skeletons from Roman Period Egypt using basiocciput osteometrics, Int. J. Osteoarchaeol. 12 (2002) 356–363.
[69] M. Walters, M. Crew, G. Fyfe, Bone surface micro-topography at craniofacial entheses: insights on osteogenic adaptation at muscle insertions, Anat. Rec. 302 (12) (2019) 2140–2155.
[70] M. Webster, H. Sheets, A practical introduction to landmark-based geometric morphometrics, Pap. Palaeontol. 16 (2010) 163–188.
[71] M.J. Zdilla, Clival canal and clival foramen development in the fetal and infant basioccipital, Child'S. Nerv. Syst. 33 (7) (2017) 1209–1216.
[72] M.J. Zdilla, J.P. Pancake, M.L. Russell, A.W. Koons, Ontogeny of the human fetal, neonatal, and infantile basioccipital bone: traditional and extended eigenshape geometric morphometric analysis, Anat. Rec. 305 (11) (2021) 3230–3242.
[73] Q. Zhang, H. Wang, J. Udagawa, H. Otani, Morphological and morphometric study on sphenoid and basioccipital ossification in normal human fetuses, Congenit. Anom. 51 (3) (2011) 138–148.
[74] W.H. Zhang, W.C. Yen, A new bony canal on the clival surface of the occipital bone, Acta Anat. 128 (1) (1987) 63–66.
[75] M.P. Zumpano, J.T. Richtsmeier, Growth-related shape changes in the fetal craniofacial complex of humans (Homo sapiens) and pigtailed macaques (Macaca nemestrina): a 3D-CT comparative analysis, Am. J. Phys. Anthropol. 120 (2003) 339–351.